Microelectronics Reliability 70 (2017) 41–48

Contents lists available at ScienceDirect

Microelectronics Reliability

journal homepage: www.elsevier.com/locate/microrel

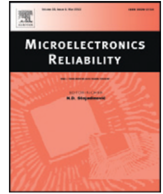

Nanocrack formation in AlGaN/GaN high electron mobility transistors utilizing Ti/Al/Ni/Au ohmic contacts

P.G. Whiting [a,*], N.G. Rudawski [a], M.R. Holzworth [a], S.J. Pearton [a], K.S. Jones [a], L. Liu [b], T.S. Kang [b], F. Ren [b]

[a] Department of Materials Science and Engineering, University of Florida, Gainesville, FL 32611-6400, United States
[b] Department of Chemical Engineering, University of Florida, Gainesville, FL 32611-6005, United States

ARTICLE INFO

Article history:
Received 25 June 2014
Received in revised form 7 February 2017
Accepted 7 February 2017
Available online 13 February 2017

Keywords:
AlGaN/GaN
High electron mobility transistor
Failure analysis
Fib/SEM
Tem
Alloyed contacts

ABSTRACT

AlGaN/GaN HEMTs are poised to become the technology of choice in RF and power electronics applications where high operating frequencies and high breakdown voltages are required. The alloyed contacting scheme utilized in the formation of the source and drain contacts of these devices affects the conduction of electrons through the 2DEG from the moment of ohmic contact formation onward to operation in the field. Analysis of the ohmic contacts of as-fabricated and electrically stressed AlGaN/GaN HEMTs, via chemical deprocessing and Scanning Electron Microscopy, indicates the presence of cracks oriented along the [11-20] directions, which nucleate at metal inclusions present under the alloyed ohmic source/drain contact metal. Cracks which form at the edges of these contact regions can extend into the channel region. It appears that electrical biasing induces additional growth in the longest cracks present within the channel regions of these devices.

© 2017 Elsevier Ltd. All rights reserved.

1. Introduction

High Electron Mobility Transistors based on Aluminum Gallium Nitride/Gallium Nitride heterostructures (AlGaN/GaN HEMTs) are poised to become the technology of choice in power electronics applications where high operating frequencies and high breakdown voltages are required [1,2]. Because of their status as an emerging technology of interest and because of materials challenges inherent in the AlGaN/GaN material system, HEMTs formed from these materials still suffer from reliability issues [3,4]. In order for these devices to mature and find widespread application, a variety of processing and integration challenges must be addressed.

One factor which is of great interest in the fabrication of AlGaN/GaN HEMTs is the access resistances associated with the source and drain electrodes. Ohmic contact formation to the source and drain electrodes can be accomplished in a variety of ways, including via implantation-induced trap assisted tunneling [5], by microwave annealing [6], or by rapid thermal annealing [7,8]. In the case of microwave or rapid thermal annealing, the formation of an ohmic contact is accomplished via the formation of an intermetallic alloy. The formation of this alloy generates metal-nitride inclusions which short out the semi-insulating AlGaN layer, allowing a direct connection to the two dimensional electron gas (2DEG) at the buried AlGaN/GaN interface which acts as the conducting channel of the HEMT. Although the 2DEG is degraded near this inclusion, a sufficient carrier density is present to enable thermionic emission [9]. When this contacting occurs, a high resistance Schottky contact at the interface between the source/drain and the AlGaN is replaced with a low resistance ohmic contact at the 2DEG.

The alloyed contact is formed from multiple metal layers which are deposited using sputtering or evaporation techniques. Ti is the metal of choice for the reactive layer which is deposited in direct contact with the AlGaN because it reacts with AlGaN to form TiN [10]. In AlInN/GaN HEMTs, this layer pushes Ga out to form an inclusion [11], and one can assume that a similar process occurs in AlGaN/GaN HEMTs as well. Au is used as a chemically inert capping layer for the contact, which prevents the oxidation of the Ti [12]. Usually, a layer of Al is deposited on top of the Ti in order to improve surface morphology after annealing.

This Al can react during annealing with Ti to form $AlTi_2N$ [13] or with Au to form $AlAu_4$ [14]. Also, because of a miscibility gap between Au and other transition metals, a reordering can occur during contact annealing wherein Au migrates to the surface of the AlGaN to replace the Ti, reducing interfacial energy at the AlGaN interface [15]. For this reason, a diffusion barrier layer is employed to prevent the reaction of Au with the layers of Al and Ti. This layer can be formed from a variety of metals, including Ni [16], Ti [17], Mo [18], Pd [19], but intermetallic reactions between the Au and this layer can reduce its efficacy [20]. Recently, diffusion barriers formed from graphene have shown promise in this application [21].

The reactions associated with alloying of these ohmic contacts result in a dramatic local modification to the semiconducting material layers

* Corresponding author.
E-mail address: patrick.g.whiting@intel.com (P.G. Whiting).

http://dx.doi.org/10.1016/j.microrel.2017.02.005
0026-2714/© 2017 Elsevier Ltd. All rights reserved.

and the surface roughness of the ohmic contacts [22]. Migration of metal outside of the ohmic contacting region and into the channel is also a concern [23]. Previous studies have already shown that this contacting scheme affects the quality of the 2DEG under the ohmic contact regions. Given the amount of material being displaced, it seems likely that local strain fields would be formed which will also influence the overall reliability of devices utilizing this contacting scheme. A study of the physical defects present in AlGaN/GaN HEMT devices as a result of alloyed contact formation seems absolutely necessary, both in as-formed devices as well as in devices where electrical biasing is applied over an extended period.

2. Experimental methods

For each device studied as part of this work, a Fe-doped GaN buffer layer was grown on a 6H-SiC substrate via Metal-Organic Chemical Vapor Deposition (MOCVD) to a thickness of approximately 2.25 μm, forming a reasonably stress-free layer and trapping most crystallographic defects formed in the GaN buffer layer [24]. A ~15 nm-thick layer of $Al_{0.28}Ga_{0.72}N$ with an n-type GaN capping layer was grown on the epitaxial GaN layer via MOCVD [25]. The resultant carrier concentration, sheet resistance, and mobility of the 2DEG formed for the device were 1.06×10^{13} cm^{-2}, 310 Ω/sq, and 1900 cm^2/V-s [26]. Further details regarding semiconductor epilayer growth are described elsewhere [27–29]. Ohmic contacts consisting of Ti/Al/Ni/Au were deposited and patterned on the surface. After patterning, these contacts were annealed for 30 s at 850 °C to improve conductivity, resulting in a contact resistance of 0.3 Ω-mm [30]. The gate contact consisted of an approximately 20 nm-thick Ni liner layer deposited directly on the n-GaN cap [31], followed by a thicker capping layer of Au. T-gates structures with gate lengths of approximately 100 nm were used in this work [30]. Finally, a 100 nm-thick SiN_x passivation layer was deposited via Plasma Enhanced Chemical Vapor Deposition (PECVD).

Devices analyzed as part of this study were primarily observed in an as-formed state. However, one device did undergo electrical stressing. Prior to stepped stressing on a representative device, the I_{DS} family of curves was taken over a V_{DS} range of 0 V to 13 V and with V_{GS} varying from −5 V to 1 V in 1 V increments. The gate electrode was then swept from $V_{GS} = -6$ V to $V_{GS} = -2$ V with $V_{DS} = 0$ V and with I_{GS} recorded, in order to determine the gate current in the reverse biased and forward biased modes of operation. Stepped stressing was performed at a temperature of 297 K on one device as part of this study, where the device was electrically step-biased from a potential of VGS = −10 V to VGS = −42 V at a rate of −1 V/min with a constant potential applied to the source and drain electrodes; VDS = 15 V. A total time under stress for the device can be assumed to be roughly equal to 32 min. At the end of off-state stressing, the family of curves for the device was generated a second time to determine the level of I_{DS} degradation after stressing. The gate electrode was, again, swept from $V_{GS} = -6$ V to $V_{GS} = -2$ V with $V_{DS} = 0$ V with I_{GS} recorded, in order to determine the gate current in the reverse biased and forward biased modes after stressing. All stressing and measurement of device characteristics was accomplished via the use of an HP4146C semiconductor parameter analyzer, capable of independent measurements of current and voltage on all three device contacts, and a Techtronix 370A curve tracer.

Lamellae for cross-sectional TEM analysis were formed via dual-beam Focused Ion Beam milling (FIB)/Scanning Electron Microscopy (SEM) on a FEI DB235, where in-situ sample milling, lift out, mounting, and thinning were accomplished via the use of an Omniprobe micromanipulator formed from W. All samples were coated with a thermally evaporated C layer 200 nm thick. Organometallic Pt was used to form the 2 μm protective mask utilized during milling with a Ga ion beam. Analysis of lamellae formed via FIB/SEM was performed on a JEOL 2010F TEM with an Energy Dispersive Spectroscopy (EDS) attachment. Deprocessed samples were studied using top-down SEM on the same FEI DB235 in Ultra High Resolution (UHR) mode with the Through Lens Detector selected.

Deprocessing begins with an exposure to hydrofluoric acid (HF) in the form of buffered oxide etch (BOE) with a 6:1 stoichiometric ratio of HF to Ammonium Fluoride (NH_4F). BOE etching occurred for a total of 15 min, during which time the PECVD SiN_x passivation layer was dissolved. With the SiN_x removed, the metallic electrodes could be removed to fully expose the surface of the AlGaN epitaxial layer. This was accomplished via a 96 h exposure in a ferric cyanide (FeCN)/potassium iodide (KI) etch solution, known as TFAC, which is commercially available from Transcene Company, Incorporated. The KI component of this etch solution actively attacks and dissolves any metal, except platinum, with perfect selectivity to the AlGaN layer below. No etch-related defects have been observed in the AlGaN as a result of etching with TFAC, which compares favorably from previous results using Aqua Regia to remove the metal layers [32]. A second etch in 6:1 HF:NH_4F was performed to remove residual SiN_x masked by the overhang of T-gate structures. Additional solvent treatments were used to eliminate all organic contaminants from the surface of the deprocessed devices, starting with a 2 h exposure in a 1:1 mixture of n-heptane and acetone, which was used to dissolve and break up the bulk of the organic film in preparation for an additional 2 h exposure in methanol. This left a pristine, but hydrophobic AlGaN surface, which was very effective at attracting dust present in the processing environment. The last step in the solvent cleaning process was a 2 h ultrasonication in water, which further cleaned the sample and also generated a hydrophillic surface ideal for imaging with SEM.

3. Results and discussion

Fig. 1 is a low magnification cross-sectional STEM image of the HEMT structure. The layered Ti/Al/Ni/Au ohmic contacts at the Source and Drain are readily visible Fig. 2(a) is a higher magnification image of a metal inclusion formed in the same HEMT under the ohmic contact which forms the source electrode as a result of the RTA process which was previously described. The top of the HAADF-STEM image in Fig. 2(a) is representative of the metal pad utilized in forming ohmic contacts of the source and drain. Visible within this metal layer are columnar grains of a TiN phase observed in the reaction pits that form upon RTA of the ohmic contacts. In some regions, TiN clearly penetrates

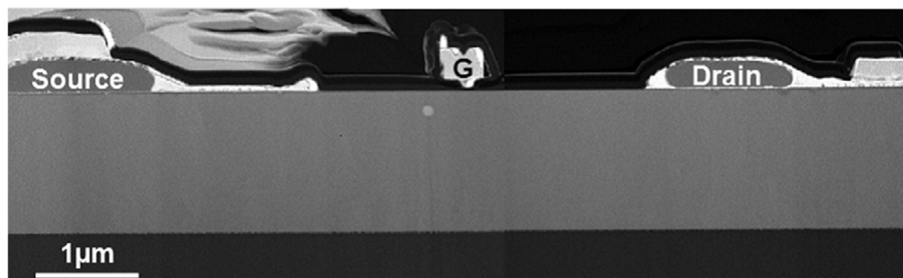

Fig. 1. A low-magnification STEM cross-section of a T-gate AlGaN/GaN HEMT.

through the AlGaN surface layer, through the 2DEG, and into the underlying GaN.

A threading dislocation extends from the bottom surface of this metal inclusion into the GaN and is marked with an arrow. The presence of this threading dislocation under the metal inclusion is consistent with previous reports regarding the annealing of metal contacts on AlGaN/GaN epitaxial structures. It has been proposed that metal inclusions form by the diffusion of metal atoms down threading dislocations, where the activation energy for diffusion is reduced. The AlGaN and GaN are not capable of supporting the high metal concentrations within these threading dislocations as metal diffusion proceeds, resulting in the formation of an inclusion rather than a metal-rich "pipe" within the AlGaN/GaN [22,33].

It is worth noting that several distinct layers of material are observable within this metal inclusion, as shown in the EDS linescan of that inclusion in Fig. 2(b). The Ti Kα, Al Kα and Ga Kα peaks highlighted in the EDS linescan indicate that the inclusion is comprised largely of titanium – likely in the form of TiN, given the observations made by previous researchers. Gallium is conspicuously absent from this inclusion and has likely been displaced. An aluminum-rich layer (most likely AlN given the need for a tunneling barrier associated with thermionic emission) is also observed. This layer was almost certainly formed by the aluminum which made up the surrounding AlGaN layer displaced by the inclusion. The observed displacement of Ga and Al by the inclusion is commensurate with studies of inclusions in AlInN [9].

Fig. 3(a) shows the ohmic contact region after deprocessing in a top-down SEM view. At least 10% of the total areal density of the source and drain regions is comprised of regions where metallic reactions resulted in inclusions. The average size of these inclusions is 62 nm across and the inclusions are hexagonally faceted, not rounded. The highly reacted source and drain surfaces are separated by a smooth AlGaN surface which comprises the channel region including the gate of the device as shown in Fig. 3(b). It should be noted that the region where the metal gate contacts the AlGaN remains unreacted because the thermal annealing process, which induces alloying, occurs prior to gate contact deposition.

A consequence of the formation of these inclusions is the generation of nanoscale cracks, as shown in Fig. 3(a) which appear to radiate from the corners of the TiN metal into the surrounding volume of the AlGaN. The sharp faceted corners of these metal inclusions appear to be very

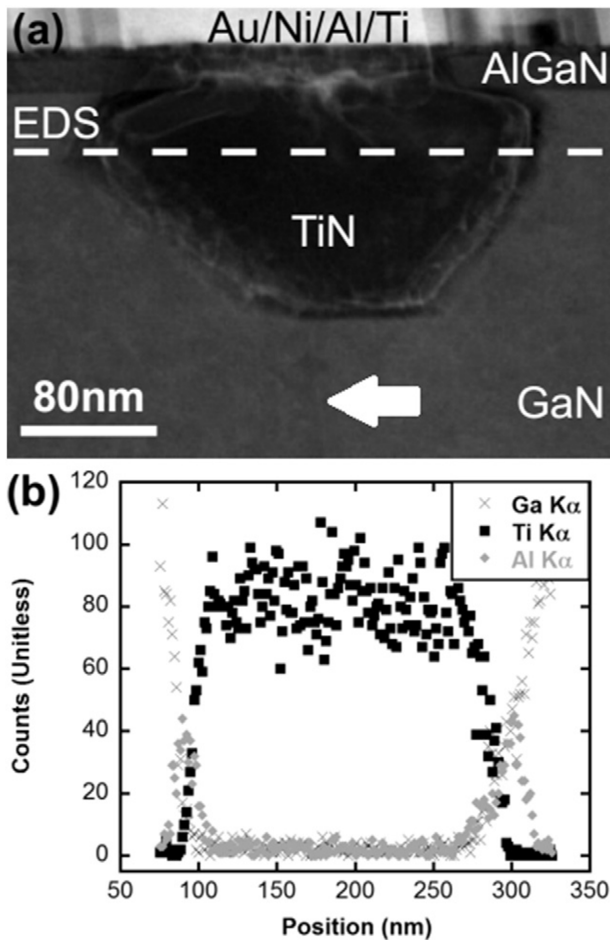

Fig. 2. a) HAADF-STEM of a TiN metal inclusion formed as the result of annealing of the Ti/Ni/Al/Au metal stack at 850 °C for 30 s in an RTA. The TiN penetrates the GaN of the HEMT through the MOCVD-grown AlGaN layer. A dotted line, marking the position of an EDS linescan performed on the inclusion, is visible. The threading dislocation which formed a pathway for metal diffusion and inclusion formation is marked with an arrow. b) The EDS spectra resulting from Ti, Al, and Ga are plotted as a function of position along the horizontal linescan. EDS analysis indicates that Ga is not present within the inclusion and that an Al pile-up occurs at the inclusion interface.

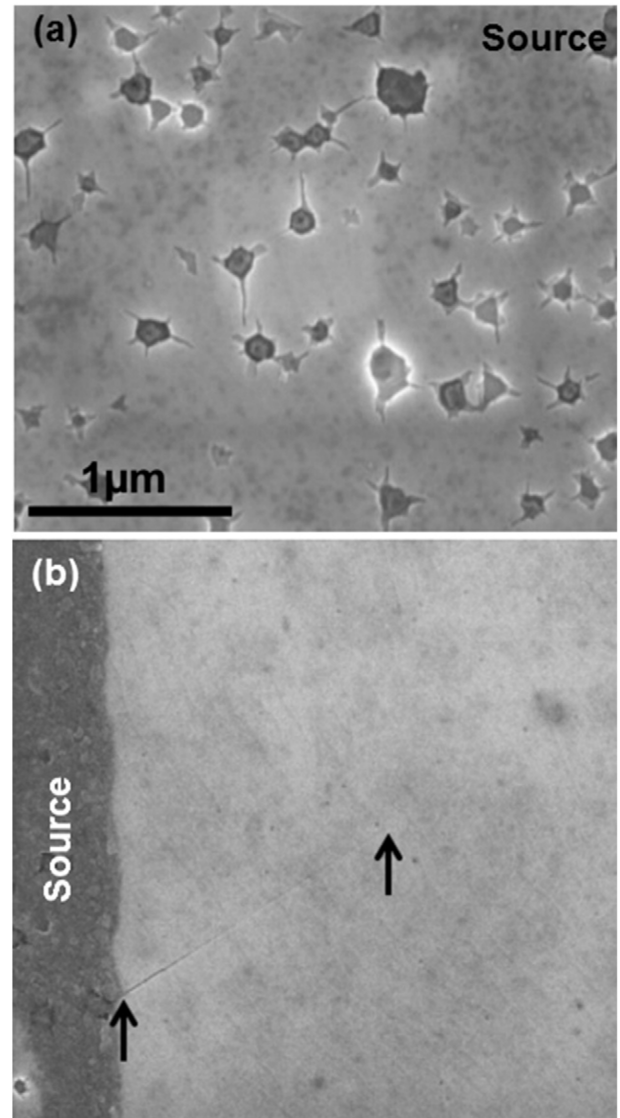

Fig. 3. a) SEM micrographs were taken of the ohmic contacts as well as the channel regions of a HEMT device recieved as-fabricated and deprocessed utilizing wet chemistry. b) Micrographs of the ohmic contacting regions of the HEMT reveal the presence of nanocracks radiating out from the pits formed by the formation and subsequent etching of TiN metal inclusions. These cracks are assumed to be present prior to deprocessing. Micrographs of the channel region of the HEMT reveal that, when cracks form at the periphery of the ohmic contacts, these features may extend into the channel region of the device.

effective in inducing the initial formation of a surface defect. The average length of one of these nanocracks is 52 nm.

Some cracks extend into the channel, as shown in Fig. 3(b), when they propagate from an inclusion at the edge of the ohmic contact. A much smaller number of inclusions exist within close proximity to the channel in comparison to the number of inclusions in the ohmic contacts, where alloying occurs. Consequently, only a small number of cracks extend into the same region. Cracks present in the channel region are, on average, longer than cracks present within the ohmic contact regions, with an average length of 273 nm.

Cross-sectional TEM was performed on a nanocrack which was observed in UHR SEM. This was accomplished by, first, marking off the crack with fiduciaries which allowed for proper orientation of the ion beam and associated lamella formed via FIB after the surface of the sample was coated in carbon. This allowed for a cross-section to be formed which runs perpendicular to the direction in which the crack was propagating. An image of this nanocrack and the corresponding orientation of the nanocrack is shown in Fig. 4(a). The resulting cross-section of the extended nanocrack was imaged using HR-XTEM as well as conventional electron diffraction utilizing a parallel beam, as shown in Fig. 4(b).

The bulk of this nanocrack is present in the AlGaN epitaxial layer and the total crack depth can be estimated to be equal to 20–30 nm. It does not extend deeply into the GaN and the aspect ratio of the crack is over 10 to 1 length to depth. This crack depth is smaller than the metal inclusions which form the cracks in the first place. Thus, the features observed in SEM appear to be “channel cracks” forming in and more or less constrained to the thin film of epitaxial AlGaN present on top of the GaN, although they do penetrate through the 2DEG interface and into the GaN. Electron diffraction taken from the AlGaN crystal region of the TEM cross-section demonstrates that the crack itself propagates along the [11–20] prism planes of the lattice. This is to be expected given the fact that cracks observed in the channel region of these devices are consistently parallel or at 60° angles to the channel edge, which is intentionally oriented normal to the prism planes of the hexagonal lattice as part of device processing. It should be noted that crack propagation has been observed along these prism planes by previous studies as a result of epitaxial film growth well beyond the pseudomorphic limit [34].

The bimodal length of nanocracks inside and outside of the ohmic contacts can be readily explained by considering the nature of the cracking which is occurring in the epitaxial layer under the channel and under the ohmic contacts. For this analysis, the assumption is made that AlGaN and GaN share a very similar Young's Modulus and Poisson's Ratio. This assumption has been made by researchers in the past when analyzing channeling cracks [35] and the assumption that the fracture toughness of bulk AlGaN is similar to that of GaN also seems reasonable, given this knowledge.

A variety of stresses act upon cracks which form in the AlGaN. These stresses can include residual stresses induced in the layer as a result of epitaxy below the pseudomorphic limit, residual stresses resultant from thin film deposition, stress due to the application of an electric field to the HEMT as a result of the inverse piezoelectric effect, and stress due to the thermal processing of the ohmic contacts and the resultant formation of a metal inclusion. It should be noted that the stresses resultant from thermal expansion coefficient mismatches are comparatively small: less than one hundred MPa even during RTA at 850 °C and significantly smaller during HEMT operation during off-state stressing, where the temperature is much lower. Thus, thermal stresses are ignored in the first-order model proposed below. A crack which forms at the edge of an ohmic contact, in the channel, will be influenced primarily by the residual epitaxial stress as well as the residual stress imposed upon the AlGaN by the passivation layer deposited above. This crack will propagate until the length of the crack is such that the residual tensile stress cannot promote additional crack formation at the tip.

The effect described above can be modeled by a modified form of Griffith's Equation [36], expressed below in Eq. (1). In this equation, K

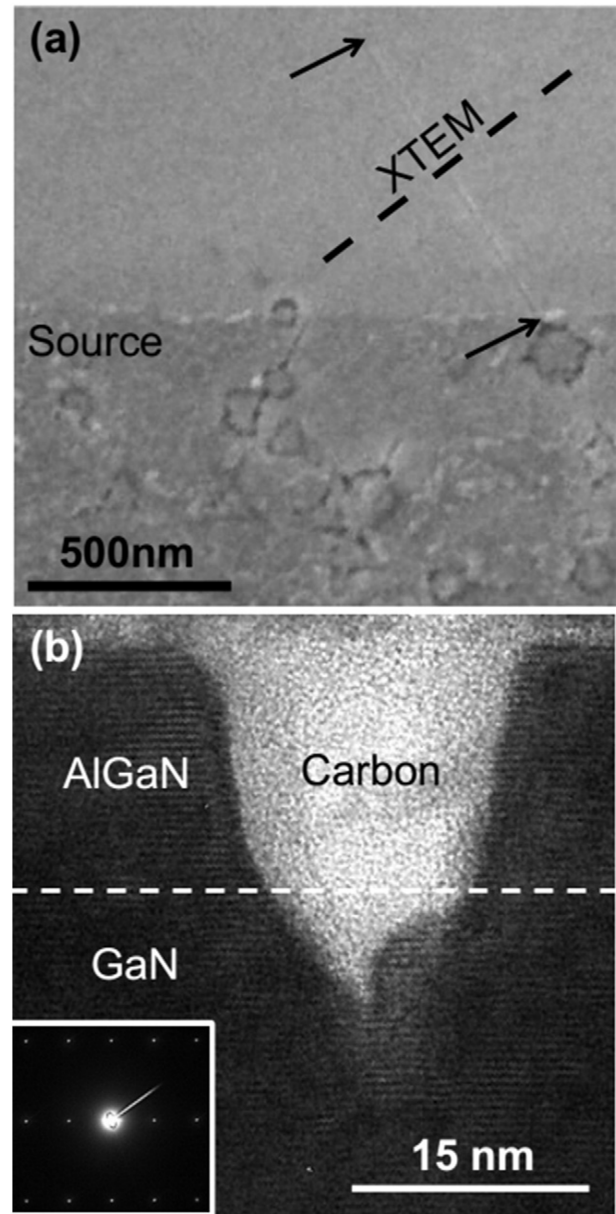

Fig. 4. a) A crack observed in the channel region after deprocessing of the device, which appeared to initially form at the periphery of the ohmic contact, was marked off with fiduciary features and cross-sectioned via FIB/SEM after a protective carbon layer was deposited on the surface. b) Analysis of the cross-sectioned nanocrack was performed using a combination of HR-XTEM and conventional electron diffraction. This analysis reveals that the majority of the crack volume exists in the MBE-grown AlGaN layer and does not extend deeply into the GaN. Furthermore, electron diffraction demonstrates that the bisected crack propagates along the [11–20] direction.

is the fracture toughness of the film (in Pa-m$^{1/2}$), c is the crack length (in m), and the tensile stress acting on the film required for additional crack growth is σ (in m). The crack length can be correlated to the stress state of the AlGaN comprising the channel region of the device, provided that the geometry of the epitaxial film is taken into account. In this case, a modifier (Z) is used to account for the geometry of a crack forming in an epitaxial film on top of a much thicker substrate. This constant approaches a value of 1.976 for a 2D channeling crack as the film becomes thinner, becoming nearly indistinguishable from this value roughly after a ratio of 1:10 is achieved between the film thickness and the thickness of the relaxed layer below it (i.e the ratio of AlGaN thickness to GaN thickness), which is certainly the approximate case for the

AlGaN epitaxial layer on top of GaN [37].

$$\sigma = K/(Z\pi c)^{1/2} \quad (1)$$

It is noted that the scenario detailed above is not exactly the physical case in the device under stress, which is coated with a passivating nitride film. However, because the constant resulting from any channeling crack in a thin film varies only between 1 and 2, this approximation is assumed to be accurate to a first order.

In order to calculate the stress present in the film from a given crack length, the fracture toughness must be estimated. Eq. (2) calculates the fracture toughness in the plane strain state. In this equation, γ is the surface energy of the crack (equal to twice the surface energy of a [11–20] prism plane, or 157 eV/$Å^2$, estimated by linear interpolation between the theoretically calculated surface energies of the GaN [11–20] and the AlN [11–20] planes) [38,39]. The Young's Modulus (E) is assumed to be equal to 309 GPa [40] and the Poisson Ratio (v) is assumed to be equal to 0.51 [35].

$$K = \left(\frac{2E\gamma}{1-v^2}\right)^{1/2} \quad (2)$$

The histogram of two distributions of crack lengths, inside and outside the channel region of the device, is shown in Fig. 5(a). This same distribution is re-expressed in terms of tensile stress derived from Griffith's Equation in Fig. 5(b). The distributions themselves are representative of approximately 600 cracks present under the ohmic contact regions and 600 cracks present under the channel regions. The 600 cracks present in the channel region originated from 20 devices received as-fabricated. Each device was 1500 μm long with a source and drain contact from which cracks could propagate, for a total nucleation perimeter of 3000 μm per device. From this, we can estimate that one crack will appear in the channel of these devices for every 100 μm of ohmic contact length. The histograms in Fig. 4 demonstrate that neither distribution is statistically normal, but rather skewed towards larger crack lengths. This skew intensifies dramatically in the case of cracks observed in the channel region, where the maximum is located around 140 nm, compared to a maximum of 50 nm for cracks observed in the ohmic contacts.

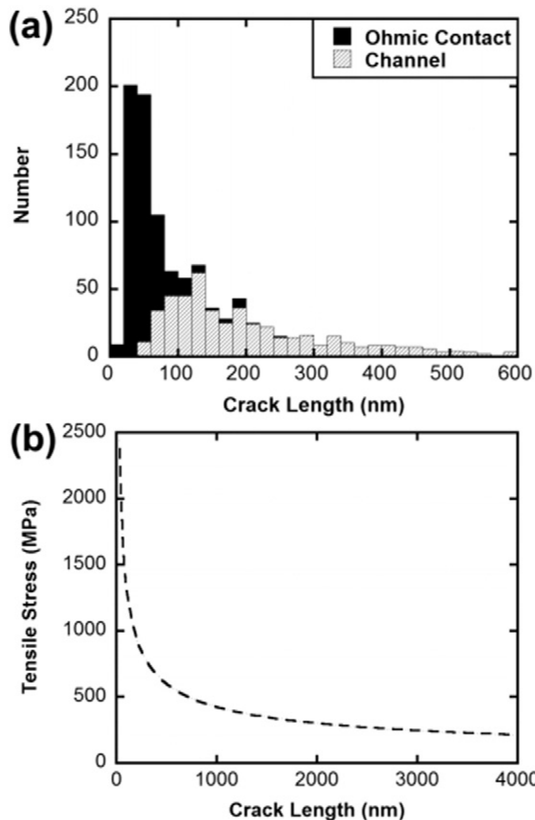

Fig. 5. a) Analysis of 600 cracks formed inside the ohmic contact regions and 600 cracks formed inside the channel regions of 10 different devices was performed using image analysis software. The lengths of the cracks observed were collated into 20 nm increments and are presented in a resulting histogram. b) A modified form of Griffith's Equation may be used to deduce the tensile stress required to induce additional crack growth for a channel crack of given length propagating through the AlGaN. By comparing this tensile stress to the maximum of the distribution of cracks present in the channel, a rough estimate can be made of the residual stress induced by AlGaN epitaxy below the pseudomorphic limit.

The maximum of the length distribution for nanocracks present within the channel region of the device yields an estimate of 780 MPa for the stress in the AlGaN film required for additional crack growth. This is approximately 40% of the calculated theoretical tensile stress in the film for $Al_{0.28}Ga_{0.72}N$ present on top of pure GaN (1.94 GPa) [41], so it seems feasible that the residual stress in the AlGaN film of the channel, due to pseudomorphic mismatch as well as due to the conditions associated with the deposition of the passivation layer, could be just barely lower than this value of 780 MPa.

Using Eq. (2), the tensile stress required for additional crack growth within the ohmic contact region can be estimated as equal to 1.87 GPa, which is significantly larger than the stress required in the channel region. This indicates that the epitaxial AlGaN is under substantial compression as a result of the formation of metal inclusions. This correlates well with the x-ray spectra observed in EDS analysis of the exemplary metal inclusions shown in Fig. 1(b), where Gallium was not observed within the metal inclusion and was assumed to be pushed out into the surrounding AlGaN as a result of contact annealing.

It is this compressive radial stress which first causes the formation of the flaws from which the cracks observed in the channel grow. Flaw formation is due to a hoop stress induced by the force of this inclusion radially compressing the AlGaN epitaxial layer. The maximum compressive stress which could result in this flaw formation can be calculated using the equation below [42], where R is the approximate radius of the metal inclusion itself and set equal to 26 nm.

$$\sigma = K/HR^{1/2} \quad (3)$$

In this case, H is a constant associated with the comparative dimensions of the crack initiated by the inclusion and the size of the inclusion, itself, and never exceeds a value of 0.24, provided that the crack's size exceeds half the radius of the inclusion. This assumption is accurate for the case of cracking in the ohmic contact regions, where the average crack length is roughly equal to the inclusion radius. So, the compressive stress induced in the AlGaN by the metal inclusions and acting on the inclusions to generate hoop stress may be calculated in this fashion. This calculation results in an estimation of 38.1 GPa for the maximum compressive stress present in the ohmic contact region required for crack formation. This maximum compressive stress is only 23% larger than the theoretical compressive stress in the AlGaN layer due to an areal compressive strain of 10.0% resultant from inclusion formation, equal to 30.8 GPa. It seems theoretically plausible that the formation of TiN inclusions drives the formation of the cracks observed in the ohmic contact regions and channel regions of these devices.

It bears noting that only the most infinitesimal amount of additional tensile stress is required within the channel in order to induce additional growth in one of these cracks. It seems plausible that electrostatic stressing could induce additional crack growth by means of a biaxial tensile strain induced by the inverse piezoelectric effect. If this occurs, it likely occurs as particularly long cracks approach the gate contact, where the electric field is substantial and induces a large piezoelectric strain [4]. This must occur infrequently, as cracks which are long enough to encounter this vertical electric field exist only at the very tail end of the distribution of crack lengths.

As was stated previously, a device which underwent stepped biasing from $V_{GS} = -10$ V to $V_{GS} = -42$ V at -1 V/min and with $V_{DS} = 15$ V was deprocessed and analyzed using top-down SEM for this study. This device demonstrated a 28% reduction in I_{DS} at $V_{GS} = -2$ V and $V_{DS} = 10$ V as well as an increase in I_{GS} at $V_{GS} = -5$ V (from 1.27 nA prior to stressing to 45 μA after stressing) as a result of the off-state stressing described above. The characteristic curves resulting from the V_{DS}/V_{GS} sweep both before and after device stressing are shown in Fig. 6(a). The gate current resulting from a V_{GS} sweep from reverse bias to forward bias is shown in Fig. 6(b). Nanocracks were observed on this device, but they were not the only defects observed. Mixing at the interface between the gate electrode and the epitaxial stack, likely due to an electrochemical reaction between the gate metal, the AlGaN, and the oxygen ambient, was also observed [43].

As was stated previously, the mean diameter of the ohmic inclusions in an as-formed device is 62 nm across, with a standard deviation of 18.0 nm. After stressing, these inclusions possess a mean diameter of 67 nm, with a standard deviation of 18.1 nm. The inclusions remain hexagonally faceted, not rounded. Histograms resulting from the SEM analysis used to generate the statistics above are shown in Fig. 7(a) for an as-formed device and in Fig. 7(b) for the stressed device. It is clear that electrostatic stressing did not appear to induce any sort of inclusion growth or interdiffusion, in contrast to diffusion studies of Au-free ohmic contacts annealed and then stressed at a constant current of 500 mA/mm [44]. The maximum annealing temperature in the referenced study was 750 °C, as compared to the devices in this study, which were annealed at 850 °C. This discrepancy might account for the lack of stress-enhanced interfacial mixing at the ohmic contact.

The histogram resulting from SEM analysis of cracks present in the channel region of the stressed device is shown in Fig. 8. As is shown on this histogram, many of the crack lengths in the stressed device were much larger than crack lengths observed in other devices which were received as-formed. Recall that the tensile stress required to induce additional growth in the longest cracks observed in as-formed devices is approximately 780 MPa. Finite element analysis by other

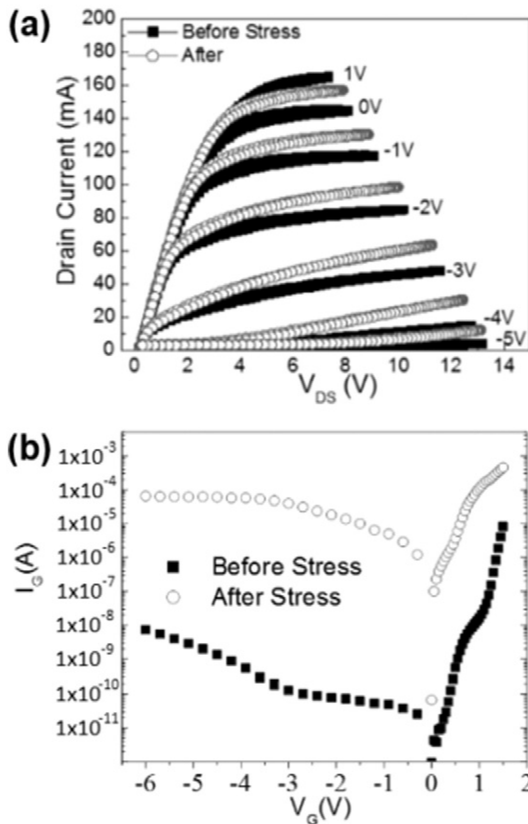

Fig. 6. a) The I_{DS} family of curves for the device under electrical analysis taken over a V_{DS} range of 0 V to 13 V and with V_{GS} varying from -5 V to 1 V in 1 V increments. The black curve represents this family of curves prior to stepped stressing from $V_{GS} = -10$ V to VGS = -42 V at a rate of -1 V/min with a constant potential applied to the source and drain electrodes; $V_{DS} = 15$ V. The grey curve represents the family of curves after stepped stressing. b) The gate current, I_{GS}, generated from sweeping from $V_{GS} = -6$ V to $V_{GS} = -2$ V with $V_{DS} = 0$ V, capturing both forward biased and reverse biased modes of operation for the Schottky diode comprising the gate contact of the device. As above, the black curve represents this I_{GS}-V_{GS} plot prior to stepped stressing from VGS = -10 V to VGS = -42 V at -1 V/min with a constant potential applied to the source and drain electrodes; $V_{DS} = 15$ V. The grey curve represents the I_{GS}-V_{GS} plot after stepped stressing.

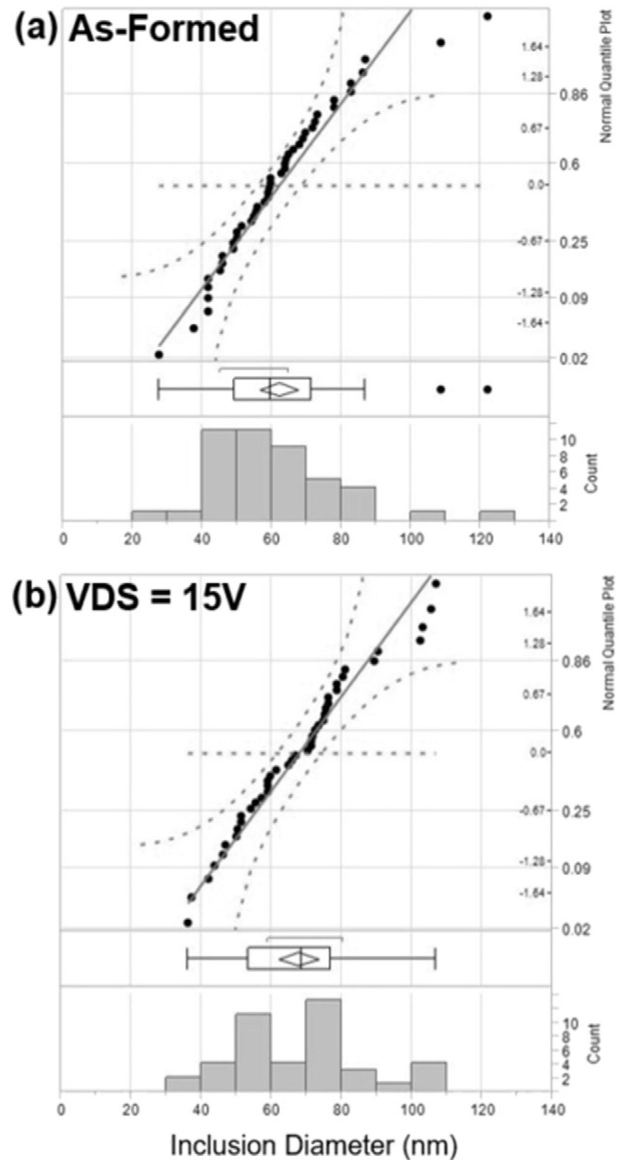

Fig. 7. a) A normal quantile plot (upper section) and histogram (lower section) resulting from SEM analysis of 44 inclusions formed as part of ohmic contact annealing at 850 °C. These inclusions were generated from a device which was deprocessed as-formed. The horizontal dotted line on the normal quantile plot indicates the 50th percentile of the distribution. The solid diagonal represents the best fit Gaussian to the data collected. The dotted curves are indicative of the 95% confidence interval for the Gaussian fit. b) A normal quantile plot (upper section) and histogram (lower section) resulting from SEM analysis of 44 inclusions formed as part of ohmic contact annealing at 850 °C. These inclusions were generated from a device which was deprocessed after stressing at $V_{DS} = 15$ V. The horizontal dotted line on the normal quantile plot indicates the 50th percentile of the distribution. The solid diagonal represents the best fit Gaussian to the data collected. The dotted curves are indicative of the 95% confidence interval for the Gaussian fit.

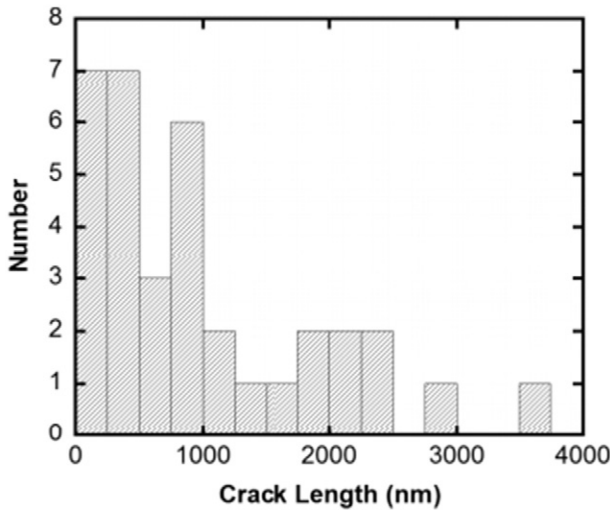

Fig. 8. The distribution of crack lengths present in a device which was stressed with V_{DS} = 15 V and V_{GS} stepped from −10 V to −42 V at a rate of −1 V/min are shown in a histogram. Cracks which were much longer than those observed in as-fabricated devices were observed.

authors has shown that residual tensile stresses can exceed 500 MPa in devices similar to the HEMTs analyzed as part of this study due to a combination of Joule heating and the inverse piezoelectric effect during pulsed on-state stressing [45], where vertical electric fields under the gate are lower than those observed in off-state stressing. It is quite possible that tensile strain in off-state stressed devices could greatly exceed 780 MPa because of higher vertical electric fields and enhanced temperatures due to shorting of the 2DEG and Ni-gate as a result of electrochemical reactions. Cracks which formed in this device as a result of processing could have been long enough to encounter strain fields which allowed them to grow longer during off-state stressing. Given that some of these cracks have bridged nearly the full length of the channel region, it seems plausible that a channel crack which extends under the gate electrode during stressing could short out the AlGaN locally if the gate metal were to refill the void formed by each channeling crack. Such a situation would fit with an increase in the gate current of the device, which has been observed previously by other authors studying microcracks with Raman spectroscopy [46] and by authors studying gate degradation under high fields [47]. It should be noted, however, that the interfacial mixing observed under the gate contact of this device could also account for this increase in I_{GS}.

The phenomenon of nanocracking in as-formed devices is not likely limited to devices similar to those observed as part of this study. Because the interfacial energy of AlGaN is reduced as it approaches AlN, its fracture toughness will also decrease. AlGaN/GaN HEMTs with higher Al content as-formed would suffer from longer channel cracks which would be more likely to encounter the gate contact of the device and grow in response to stress. Devices with larger numbers of threading dislocations available to induce inclusion formation under the ohmic contacts would also suffer from larger numbers of cracks as the density of nucleating flaws increased. As stability of the gate contact improves in HEMTs, cracking may become a more dominant mechanism in their degradation and its specific electrical fingerprint may be more readily observed.

There are ways in which cracking could be mitigated. Obviously, reducing Al content in the AlGaN epilayer is one solution (via an increase in fracture toughness), but this would have adverse effects on the 2DEG of the HEMT. Adopting an epilayer material with higher fracture toughness might be a more attractive option. By reducing the number of threading dislocations present in the AlGaN epilayer and increasing the thermal budget of annealing, the average area of the TiN inclusions and their associated radius of curvature could be increased. This would reduce the hoop stress under the ohmic contact and could conceivably reduce the number of cracks formed at the edge of the channel. Another feasible option would be to increase the residual compressive stress locally at the ohmic contact without inducing additional hoop stress via the deposition of a thin film. Arguably the best option for reducing the formation of nanocracks is to use an active metal for ohmic contacting which can form a metal-nitride inclusion in which Ga and Al are soluble in order to reduce compression and associated hoop stress in the ohmic contact region or in using a contacting scheme which does not employ the formation of metal inclusions in the first place.

4. Conclusions

Analysis of the ohmic contacts of as-fabricated and electrostatically stressed AlGaN/GaN HEMTs indicates the presence of nanocracks oriented along the [11–20] directions. These cracks nucleate at metal inclusions present under the alloyed ohmic contact metal as a result of a hoop stress which accompanies the biaxial compressive stress induced in the AlGaN as a result of the formation of these inclusions during contact annealing. Cracks which form at the edges of these contact regions can extend into the channel region, where a 780 MPa residual tensile stress exists due to the thin film processing of the HEMT. It stands to reason that long cracks which bridge the channel region of the device can be avoided through the proper selection of epilayer thicknesses and crystal quality as well as thin film passivation materials.

Electrostatic stressing could be capable of inducing additional growth in the longest cracks present within the channel regions of these devices, which make the closest approach to the gate electrodes of these devices. The evidence presented in this study suggests that cracks may grow in the presence of large vertically-oriented electric fields, which induce biaxial strain fields within the AlGaN. It seems plausible that cracks which extend under the gate electrode of the device undermine the rectifying nature of this contact. It should be noted, however, that the results in this study which suggest that electrostatic stressing may induce nanocrack growth come from a single device; certainly not a statistically significant dataset. While cracks were observed in similar devices observed in other studies which the authors have performed, these cracks did not exhibit the extreme elongation observed on the stressed device analyzed as part of this study, but were similar to cracks observed in as-formed devices. It should be noted, however, that these studies were undertaken at very different stressing conditions [32].

While the results of this study are intriguing, further study of the phenomenon is necessary before any definitive statement can be made as to the mechanisms which give rise to this particular defect under electrostatic stress conditions. Chief amongst the desired outcomes of such a study would be the direct observation via TEM of channel crack propagation under the gate contact of a HEMT and a correlation to electrical degradation of the device. It seems plausible that HF-based deprocessing without the use of TFAC or aqua regia could be used to detect cracks without damaging the gate contact of the device. This would allow a FIB engineer to use the gate metal of the device as a protective mask to form a lamellar cross-section for TEM to enable direct imaging of the nanocrack under the gate.

Acknowledgments

The authors acknowledge the Air Force Office of Scientific Research and the Multidisciplinary University Research Initiative program for funding this research per grant number FA9550-08-1-0264. The Major Analytical Instrumentation Center at the University of Florida is acknowledged for use of the focused ion beam/scanning electron microscope and transmission electron microscope facilities.

References

[1] E.O. Johnson, Physical limitation on frequency and power parameters of transistors, RCA Rev. 163–176 (1965).
[2] S.T. Sheppard, K. Doverspike, W.L. Pribble, S.T. Allen, J.W. Palmour, L.T. Kehias, T.J. Jenkins, High-power microwave GaN/AlGaN HEMTs on semi-insulating silicon carbide substrates, IEEE Elec. Dev. Lett. 20 (1999) 161–163.
[3] G. Menghesso, Reliability of GaN high-electron-mobility transistors: state of the art and perspectives, IEEE Trans. Device Mater. Reliab. 8 (2008) 332–344.
[4] J. DelAlamo, J. Joh, GaN HEMT reliability, Microelectron. Reliab. 49 (2009) 1200–1206.
[5] P. Upadhyay, M. Meer, K. Takhar, D. Khachariya, A.S. Kumar, D. Banerjeee, S. Ganguly, A. Laha, D. Saha, Improved ohmic contact to GaN and AlGaN/GaN two-dimensional electron gas using trap assisted tunneling by B implantation, Phys. Status Solidi B 252 (5) (2015) 989–995.
[6] L.Q. Zhang, J.S. Shi, H.F. Huang, X.Y. Liu, S.X. Zhao, P.F. Wang, D.W. Zhang, Low-temperature ohmic contact formation in GaN high electron mobility transistors using microwave annealing, Elec. Dev. Lett 36 (9) (2015) 896–898.
[7] Q. Feng, L.M. Li, Y. Hao, J.Y. Ni, J.C. Zhang, The improvement of ohmic contact of Ti/Al/Ni/Au to AlGaN/GaN HEMT by multi-step annealing method, Solid State Electron. 53 (2009) 955–958.
[8] M.E. Lin, Z. Ma, F.Y. Huang, Z.F. Fan, L.H. Allen, H. Morkoc, Low resistance ohmic contacts on wide band-gap GaN, Appl. Phys. Lett. 63 (1993) 1003–1005.
[9] S. Kim, J.H. Ryou, R.D. Dupuis, H. Kim, Carrier transport mechanism of low resistance Ti/Al/Au ohmic contacts to AlInN/GaN heterostructures, Appl. Phys. Lett. 102 (2013) 052107.
[10] A.N. Bright, P.J. Thomas, M. Weyland, D.M. Tricker, C.J. Humphreys, R. Davies, Correlation of contact resistance with microstructure for Au/Ni/Al/Ti/AlGaN/GaN ohmic contacts using transmission electron microscopy, J. Appl. Phys. 89 (2001) 3143.
[11] F. Iucolano, G. Greco, F. Roccaforte, Correlation between microstructure and temperature dependent electrical behavior of annealed Ti/Al/Ni/Au ohmic contacts to AlGaN/GaN heterostructure, Appl. Phys. Lett. 103 (2013) 201604.
[12] L. Wang, F.M. Mohammed, I. Adesida, Formation mechanism of ohmic contacts on AlGaN/GaN heterostructures: electrical and microstructure characterizations, J. Appl. Phys. 103 (2008) 093516.
[13] F. Roccaforte, F. Iucolano, F. Giannazzo, A. Alberti, V. Raineri, Nanoscale carrier transport in Ti/Al/Ni/Au ohmic contacts on AlGaN epilayers grown on Si(111), Appl. Phys. Lett. 89 (2006) 022103.
[14] L. Zhou, M.R. Johnson, D.J. Smith, D.J. Meyer, D.F. Storm, D.S. Katzer, B.P. Downey, Microstructure of Ti/Al/Ni/Au ohmic contacts for N-polar GaN/AlGaN high electron mobility transistor devices, J. Vac. Sci. Technol. B. 32 (2014) 011201.
[15] R. Maeta, H. Tokuda, M. Kuzuhara, Formation of low ohmic contacts to AlGaN/GaN heterostructures using Ti/Al-based metal stack, IEEE Meeting for Fut. Elec. Dev, June 5–6, 2013.
[16] R. Gong, J. Wang, S. Liu, Z. Dong, M. Yu, C.P. Wen, Y. Cai, B. Zhang, Analysis of surface roughness in Ti/Al/Ni/Au ohmic contacts to AlGaN/GaN high electron mobility transistors, Appl. Phys. Lett. 97 (2010) 062115.
[17] J. Chen, D.G. Ivey, J. Bardwell, Y. Liu, H. Tang, J.B. Webb, Microstructural analysis of Ti/Al/Ti/Au ohmic contacts to n-AlGaN/GaN, J. Vac. Sci. Technol. A 20 (2002) 1004.
[18] L. Zhou, L.H. Leach, X. Ni, H. Morkoc, J.D. Smith, Ti/Al/Ni/Au contacts for AlInN/AlN/GaN-based heterojunction field-effect transistors, J. Appl. Phys. 107 (2010) 014508.
[19] M.W. Fay, G. Moldovan, N.J. Weston, P.D. Brown, I. Harrison, K.P. Hilton, A. Masterson, D. Wallis, R.S. Balmer, M.J. Uren, T. Martin, Structural and electrical characterization of AuPdAlTi ohmic contacts to AlGaN/GaN with varying Ti content, J. Appl. Phys. 96 (2004) 5588.
[20] B. Jacobs, M.C.J.C.M. Kramer, E.J. Geluk, F. Karouta, Optimization of a Ti/Al/Ni/Au ohmic contact on AlGaN/GaN FET structures, J. Cryst. Growth 241 (2002) 15–18.
[21] W.K. Morrow, C. Lee, S.P. DenBaars, F. Ren, S.J. Pearton, Role of graphene interlayers in mitigating degradation of Ni/Au ohmic contact morphology on p-type GaN, Vacuum 128 (2016) 34–38.
[22] N. Chaturvedi, U. Zeimer, J. Wurfl, G. Trankle, Mechanism of formation of ohmic contact formation in AlGaN/GaN high electron mobility transistors, Semicond. Sci. Technol. 21 (2006) 175–179.
[23] H.P. Xin, S. Poust, W. Sutton, D. Li, D. Lam, I. Smorchkova, R. Sandhu, B. Heying, J. Uyeda, M. Barsky, M. Wojtowicz, R. Lai, Optimization of AlGaN/GaN HEMT ohmic contacts for improved surface morphology with low contact resistance, CS MANTECH Conference, 2010.
[24] S. Kolluri, S. Keller, S.P. DenBaars, U.K. Mishra, Microwave power performance n-polar GaN MISHEMTs grown by MOCVD on SiC substrates using an Al_2O_3 etch-stop technology, IEEE Electron Device Lett. 33 (2012) 44–46.
[25] M.A. Khan, J.N. Kuznia, J.M. Vanhove, D.T. Olson, S. Krishnankutty, R.M. Kolbas, Growth of high optical and electrical quality GaN layers using low-pressure metalorganic chemical vapor-deposition, Appl. Phys. Lett. 58 (1991) 526–527.
[26] E.A. Douglas, C.Y. Chang, B.P. Gila, M.R. Holzworth, K.S. Jones, L. Liu, et al., Investigation of the effects of temperature during off-state degradation of AlGaN/GaN high electron mobility transistors, Microelectron. Reliab. 52 (2012) 23–28.
[27] W. Nagy, J. Brown, R. Borges, S. Singhal, Linearity characteristics of microwave-power GaN HEMTs, IEEE Trans. Microw. Theory Tech. 51 (2003) 660–664.
[28] S. Singhal, T. Li, A. Chaudhari, A.W. Hanson, R. Therrien, J.W. Johnson, et al., Reliability of large periphery GaN-on-Si HFETs, Microelectron. Reliab. 46 (2006) 1247–1253.
[29] J.D. Brown, R. Borges, E. Piner, A. Vescan, S. Singhal, R. Therrien, AlGaN/GaN HFETs fabricated on 100-mm GaN on silicon (111) substrates, Solid State Electron. 46 (2002) 1535–1539.
[30] B. Luo, J. Kim, R. Mehandru, F. Ren, K.P. Lee, S.J. Pearton, et al., Comparison of ohmic contact properties on n-GaN/p-SiC and n-AlGaN/p-SiC heterojunctions, Solid State Electron. 46 (2002) 1345–1349.
[31] W.-K. Wang, P.-C. Lin, C.-H. Lin, C.-K. Lin, Y.-J. Chan, G.-T. Chen, et al., Performance enhancement by using the n^+-GaN cap layer and gate recess technology on the AlGaN-GaN HEMT fabrication, IEEE Electron Device Lett 26 (2005) 5–7.
[32] P.G. Whiting, N.G. Rudawski, M.R. Holzworth, S.J. Pearton, K.S. Jones, L. Liu, T.S. Kang, F. Ren, Under-gate defect formation in Ni-gate AlGaN/GaN high electron moblity transistors, Microelectron. Reliab. 52 (2012) 2542–2546.
[33] M. Kuball, M. Tapajna, R.J.T. Simms, M. Faqir, U.K. Mishra, AlGaN/GaN HEMT device reliability and degradation evolution: importance of diffusion processes, Microelectron. Reliab. 5 (2010) 195–200.
[34] P.J. Parbrook, D. Wang, M.A. Whitehead, C.N. Harrison, R.J. Lynch, T.R. Murray, Crack formation and development in AlGaN/GaN structures, Phys. Status Solidi C 0 (2003) 2055–2058.
[35] R. Huang, J.M. Prevost, Z.Y. Huang, Z. Suo, Channel-cracking of thin films with the extended finite element method, Eng. Fract. Mech. 70 (2003) 2513–2526.
[36] T.H. Courtney, Fracture mechanics, Mechanical Behavior of Materials, Waveland Press, Long Grove, IL 2000, pp. 404–448.
[37] S. Einfeldt, V. Kirchner, H. Heinke, M. Dieselberg, S. Figge, K. Vogeler, D. Hommel, Strain relaxation in AlGaN under tensile plane stress, J. Appl. Phys. 88 (2000).
[38] J.E. Northrup, J. Neugebauer, Theory of GaN [$10\bar{1}0$] and [$11\bar{2}0$] surfaces, Phys. Rev. B 53 (1996) R10477–R10480.
[39] D. Holec, P.H. Maryhofer, Surface energies of AlN allotropes from first principles, Scr. Mater. 67 (2012) 760–762.
[40] G. Steude, B.K. Meyer, A. Goldner, A. Hoffman, A. Kaschner, F. Bechstedt, H. Amano, I. Akasaki, Strain modification of GaN in AlGaN/GaN epitaxial films, Jpn. J. Appl. Phys. 38 (1999) L498–L500.
[41] O. Ambacher, J. Smart, J.R. Shealy, N.G. Wiemann, K. Chu, M. Murphy, W.J. Schaff, L.F. Eastman, R. Dmitrov, L. Wittmer, M. Stutzmann, W. Rieger, J. Hilsenbeck, Two-dimensional electron gas induced by spontaneous and piezoelectric polarization charges in N-face and Ga-face AlGaN/GaN heterostructures, J. Appl. Phys. 85 (1999) 3222–3234.
[42] J. Suo, Reliability of interconnect structures in comprehensive structural failure, Elsevier 8 (2003) 265–324.
[43] M.R. Holzworth, N.G. Rudawski, P.G. Whiting, S.J. Pearton, K.S. Jones, L. Lu, T.S. Kang, F. Ren, E. Patrick, M.E. Law, Field-induced defect morphology in Ni-gate AlGaN/GaN high electron mobility transistors, Appl. Phys. Lett. 103 (2013) 023503.
[44] T.-L. Wu, D. Marcon, S. Stoffels, S. You, B. De Jaeger, M. Van Hove, G. Groeseneken, S. Decoutere, Stability evaluation of Au-free Ohmic contacts on AlGaN/GaN HEMTs under a constant current stress, Microelectron. Reliab. 54 (10) (2014) 2232–2236.
[45] J.P. Jones, E. Heller, D. Dorsey, S. Graham, Transient stress characterization of AlGaN/GaN HEMTs due to electrical and thermal effects, Microelectron. Reliab. 55 (12) (2015) 2634–2639.
[46] J.W. Pomeroy, M. Kuball, D.J. Wallis, A.M. Keir, K.P. Hilton, R.S. Balmer, M.J. Uren, T. Martin, P.J. Heard, Thermal mapping of defects in AlGaN/GaN heterostructure field effect transistors using micro-Raman spectroscopy, Appl. Phys. Lett. 87 (2005) 102508.
[47] U. Chowdhury, J.L. Jimenez, C. Lee, E. Beam, P. Saunier, T. Balistreri, TEM observation of crack- and pit-shaped defects in electrically degraded GaN HEMTs, IEEE Elec. Dev. Lett. 29 (2008) 1098–1100.